Ferumoxytol Is Not Retained in Kidney Allografts in Patients Undergoing Acute Rejection

Maryam Aghighi[1], **Laura Pisani**[1], **Ashok J. Theruvath**[1], **Anne M. Muehe**[1], **Jessica Donig**[1], **Ramsha Khan**[1], **Samantha J. Holdsworth**[1], **Neeraja Kambham**[2], **Waldo Concepcion**[3], **Paul C. Grimm**[4], and **Heike E. Daldrup-Link**[1,5]

[1]Department of Radiology, Pediatric Molecular Imaging in the Molecular Imaging Program at Stanford (@PedsMIPS), Lucile Packard Children's Hospital, Stanford University School of Medicine, 725 Welch Road, Stanford, 94305, CA, USA

[2]Department of Pathology, Stanford University, Stanford, CA, USA

[3]Department of Surgery, Stanford University, Stanford, CA, USA

[4]Department of Pediatrics, Stanford University, Stanford, CA, USA

[5]Department of Pediatrics, Lucile Packard Children's Hospital, Stanford School of Medicine, 725 Welch Rd, Stanford, CA, 94305, USA

Abstract

Purpose: To evaluate whether ultrasmall superparamagnetic iron oxide nanoparticle (USPIO)-enhanced magnetic resonance imaging (MRI) can detect allograft rejection in pediatric kidney transplant patients.

Procedures: The USPIO ferumoxytol has a long blood half-life and is phagocytosed by macrophages. In an IRB-approved single-center prospective clinical trial, 26 pediatric patients and adolescents (age 10–26 years) with acute allograft rejection ($n = 5$), non-rejecting allografts ($n = 13$), and normal native kidneys ($n = 8$) underwent multi-echo T2* fast spoiled gradient-echo (FSPGR) MRI after intravenous injection (p.i.) of 5 mg Fe/kg ferumoxytol. T2* relaxation times at 4 h p.i. (perfusion phase) and more than 20 h p.i. (macrophage phase) were compared with biopsy results. The presence of rejection was assessed using the Banff criteria, and the prevalence of macrophages on CD163 immunostains was determined based on a semi-quantitative scoring system. MRI and histology data were compared among patient groups using t tests, analysis of variance, and regression analyses with a significance threshold of $p < 0.05$.

Results: At 4 h p.i., mean T2* values were 6.6 ± 1.5 ms for native kidneys and 3.9 ms for one allograft undergoing acute immune rejection. Surprisingly, at 20–24 h p.i., one rejecting allograft showed significantly prolonged T2* relaxation times (37.0 ms) compared to native kidneys (6.3 ± 1.7 ms) and non-rejecting allografts (7.6 ± 0.1 ms). Likewise, three additional rejecting allografts showed significantly prolonged T2* relaxation times compared to non-rejecting allografts at later post-contrast time points, 25–97 h p.i. ($p = 0.008$). Histological analysis revealed edema and compressed microvessels in biopsies of rejecting allografts. Allografts with and without rejection showed insignificant differences in macrophage content on histopathology ($p = 0.44$).

Conclusion: After ferumoxytol administration, renal allografts undergoing acute rejection show prolonged T2* values compared to non-rejecting allografts. Since histology revealed no significant differences in macrophage content, the increasing T2* value is likely due to the combined effect of reduced perfusion and increased edema in rejecting allografts.

Keywords

Kidney allograft rejection; MR imaging; Iron oxide nanoparticles; Ferumoxytol

---

Introduction

In patients with end-stage renal failure, renal allograft transplantation leads to markedly improved quality of life and survival when compared to chronic dialysis [1]. To date, more than 1.4 million adult patients and 70,000 children have received renal allografts globally [1, 2]. However, a major complication of renal allograft transplantation in children and adolescents is an acute or chronic rejection, which causes almost half of the allograft losses in this age group [3]. Currently, the diagnosis of rejection relies on allograft biopsies, which are invasive, require general anesthesia in children, and are prone to sampling errors. A non-invasive diagnostic test, which directly detects allograft rejection and can be used longitudinally in patients would obviate the need for invasive biopsies and anesthesia, reduce associated complications, and reduce health care costs.

Previous experimental approaches to image renal and liver allograft rejection include 99mTc-annexin V-enhanced SPECT in rats [4], [99mTc]OKT3 scintigraphy in rats [5], and Tc-99m labeled mononuclear cell scintigraphy in humans [6]. These approaches are not clinically available at this time. Other investigators used Doppler ultrasound [7] or magnetic resonance imaging (MRI) with non-specific extracellular clinical contrast agents to diagnose impaired allograft perfusion [8–11]. Kalb et al. found T2 signal elevation with rejection [12]. However, unenhanced T2-weighted images have the limitation that they are non-specific with respect to differentiating infection from immune rejection [7].

Recently, clinically applicable iron oxide nanoparticles helped to detect macrophage infiltration in acute cardiac allograft rejection in rats [13], acute pancreatic allograft rejection in rats [14], and renal allograft rejection in rats [15] and humans [16]. In renal allografts that underwent rejection, CD68-positive macrophages were present in areas of tissue-damage and fibrosis, and were prevalent in more severe forms of rejection representing an independent predictor of worse outcomes [17–19]. Previous studies show that the FDA-

approved iron oxide nanoparticle compound ferumoxytol is phagocytosed by macrophages in the liver, spleen, or tumors causing significant T2* shortening of those tissues [20–23]. We hypothesized that rejection of renal allografts would be accompanied by increased macrophage prevalence and therefore by significant T2* shortening with ferumoxytol. Thus, the goal of our study was to evaluate whether ferumoxytol-enhanced MRI could detect allograft rejection non-invasively in pediatric patients.

Materials and Methods

This HIPAA compliant study was approved by the committee on human research at our institution and was performed under an investigator-initiated investigational new drug (IND) approval with the FDA (IND 111 154) after written informed consent was obtained from the child's legal representative or the competent adult patient (Clinical Trials Identifier: NCT02006108).

We examined 26 pediatric and adolescent patients, including 8 age-matched patients with native (*i.e.*, healthy non-transplant) kidneys (mean age 19.7 ± 5.4 years), 13 with biopsy-proven non-rejecting allografts (mean age 17.8 ± 3.4 years), and 5 undergoing biopsy-proven allograft rejection (mean age 17.7 ± 1.0 years). The glomerular filtration rate (GFR) was calculated using the CKD-EPI equation [24].

MR Imaging

Investigational new drug (IND) approval was obtained from the FDA for off-label use of the iron supplement ferumoxytol (Feraheme®, AMAG Pharmaceuticals, Inc.) [25] as a MR contrast agent in pediatric patients and young adults. Ferumoxytol is composed of semi-synthetic carbohydrate-coated superparamagnetic iron oxide nanoparticles with a molecular weight of 731 kDa [26], a mean hydrodynamic particle diameter of 30 nm [27], and a plasma half-life of 14–15 h [28]. Due to superparamagnetic properties, ferumoxytol nanoparticles cause positive contrast (bright signal) on T1-weighted MR images and negative contrast (dark signal) on T2- and T2*-weighted MR images [28]. For this study, ferumoxytol was slowly infused intravenously at a dose of 5 mg Fe/kg body weight over at least 15 min, followed by MRI. Since the optimal time point for post-contrast scans is not known, post-ferumoxytol (p.i.) MRI scans were obtained at time points ranging from 1 h to 14 days. MRI exams were conducted on a 3T MRI scanner (GE Discovery MR750, GE Healthcare), using a multi-echo, flow-compensated 2D fast spoiled gradient recalled (FSPGR) sequence for depiction of renal allografts and concomitant iron detection with the following parameters: TE = 2.2 ms, inter-echo interval 2.2 ms, number of echoes per excitation 8, TR = 150 ms, flip angle = 30°, FOV = 256×256 mm^2, voxel size $1 \times 1 \times 1$ mm^3, and scan times of 8.4 ± 4.7 min. T2* maps were calculated using the Cinetool software application (GE Global Research). Mean T2* relaxation times were evaluated within manually defined regions of interest (ROIs) for the whole kidney, kidney medulla, and kidney cortex, in native, non-rejecting allograft and rejecting allograft patient groups.

Histopathology

Patients with allografts underwent routine biopsies either (a) on the same day as the MRI ($n = 12$), (b) before the MRI ($n = 3$; mean 18 days prior), or (c) after the MRI ($n = 5$; mean 10 days later). The biopsy specimens were dissected parasagittally, kept in formalin overnight, dehydrated through graded alcohol washes (70, 95, and 100 %), embedded in paraffin and sliced on a microtome. Five-micrometer thick tissue slices on glass slides were stained with hematoxylin and eosin (HE) and Periodic acid-Schiff (PAS) stains. In addition, the samples were stained with antisera against CD163 (Novocastra, Clone 10D6, 1:50 dilution, performed on the Ventana XT using HIER solution CC1, pH 8.0). The histological and immunohistochemical analysis was performed under a light microscope (Olympus BX51). The biopsy samples were evaluated for cellular and antibody-mediated rejection as per the Banff 2013 criteria [29]. Evidence for other disease processes affecting the allograft was also sought. The CD163 stained slides were scored blinded as follows: no stained cells = 0, <10 positive cells/hpf present in <25 % of biopsy = 1, >10 positive cells/hpf in 26–50 % of biopsy = 2, and >10 positive cells in >50 % of biopsy = 3.

Data Analysis

GFR and MRI data were compared between patients with non-rejecting and rejecting allografts using the two-sided t test. In addition, mean T2* values of whole kidneys as well as kidney cortex and medulla were compared between the three patient groups of native, non-rejecting and rejecting allografts using analysis of variance (ANOVA). In addition, T2* relaxation times were correlated with the CD163 score, using a linear regression analysis. All statistical computations were performed with Microsoft Excel software. An alpha level of 0.05 was chosen to indicate significant differences.

Results

The *in vivo* pharmacokinetics of superparamagnetic iron oxide nanoparticles (SPIO) in non-rejecting, acute and advanced rejecting allografts, based on our results and available literature to date [8, 30, 31] are depicted in Electronic Supplementary Material (ESM) Fig. S1.

All ferumoxytol contrast injections were uneventful with no noted adverse events. All patients tolerated the imaging procedure well, without subjective or objective side effects. One patient did not complete the study: He provided informed consent and received a ferumoxytol injection but did not come to the MRI scan due to personal reasons (this patient is not included in the patient numbers cited above).

The patients with non-rejecting allografts showed a normal GFR of 90 ± 29 ml/min/1.73 m^2, whereas patients undergoing allograft rejection had a significantly reduced ($p = 0.01$) GFR of 52 ± 24 ml/min/1.73 m^2 before ferumoxytol injection and unchanged ($p = 0.77$) GFR of 54 ± 19 ml/min/1.73 m^2 after ferumoxytol injection, using the CKD-EPI equation [24] based on measured serum creatinine values (Table 1).

T2* relaxation time maps of a native kidney without ferumoxytol, as well as of non-rejecting allografts at progressing time points after the intravenous injection of ferumoxytol, are

shown in ESM Fig. S2. As expected [32, 33], intravenous ferumoxytol injection led to an initial T2* shortening in all kidneys, likely due to its blood pool effect, followed by gradual recovery of T2* signal over time, presumably due to diminishing blood pool effect and ferumoxytol uptake in the reticuloendothelial system [34, 35].

Surprisingly, rather than having shortened T2* times as hypothesized, at 20–24 h p.i., one rejecting allograft showed significantly prolonged T2* relaxation times (37.0 ms) compared to native kidneys (6.3 ± 1.7 ms) and non-rejecting allografts (7.6 ± 0.1 ms) ($p = 0.008$) (Figs. 1, 2, and 3). For one allograft undergoing acute rejection, the mean T2* value at 4 h p.i was 3.9 ms compared with 6.6 ± 1.5 ms for the native kidney. This initial T2* shortening of both normal kidneys and rejecting allografts was presumably due to relatively high intravascular ferumoxytol concentration and resultant Bblooming^ effect during this early perfusion phase.

Histological analysis revealed interstitial expansion and glomerular vasospasm in allografts undergoing rejection (Fig. 4a, b). This would decrease ferumoxytol perfusion in rejecting allografts.

Allografts with or without acute rejection did not show significant differences in macrophage prevalence on histopathology ($p = 0.44$). Most non-rejecting allografts showed no macrophage infiltration (Fig. 4c). However, biopsies from two patients with non-rejecting allografts showed parenchymal scarring (Patient #3) and BK nephropathy (Patient #10) with abundant macrophages (Table 1 and Fig. 4d). Patients undergoing allograft rejection showed a wide range of macrophage prevalence (Fig. 4e, f). T2* values did not significantly correlate with macrophage prevalence in non-rejecting ($p = 0.12$) and rejecting allografts ($p = 0.34$; Fig. 5).

Based on the acquired results, our nephrology team generated a decision flow chart for the diagnosis of kidney transplant rejection on ferumoxytol-enhanced MR images (Fig. 6).

Discussion

Assuming that renal allografts undergoing rejection would consistently harbor increased numbers of macrophages, we hypothesized that allograft rejection would lead to increased retention of ferumoxytol and resultant T2* shortening on MR images. However, we found the opposite effect: allografts undergoing acute rejection showed prolonged T2* values on ferumoxytol-enhanced MR images. This can be explained by glomerular vasospasm, reduced perfusion, and edema of rejecting allografts as compared to non-rejecting allografts, which leads to diminished ferumoxytol perfusion. This observation is in agreement with previously reported perfusion studies with other contrast agents [9, 36, 37] (Table 2) and increased signal levels of renal allografts undergoing rejection on non-contrast T2-weighted MR scans [12] (Table 3).

Children and adolescents with kidney transplants currently undergo at least three routine biopsies during the first 2 years after a renal transplant. If at least some of these biopsies could be replaced by a non-invasive imaging test, this would benefit the patients and the health care system. This would require that an imaging test reliably excludes an allograft

rejection, such that these patients could be spared a biopsy. While both adult and pediatric patients would benefit from a non-invasive imaging approach, our investigations focused on pediatric patients. The clinical impact would be particularly high in this population because (i) many children cannot hold still for invasive procedures, so pediatric biopsies are usually done under anesthesia and adult transplant biopsies are usually done without anesthesia [47]. (ii) Adult transplants are usually retroperitoneal in location, which can be more easily accessed than pediatric transplants, which may be intra-abdominal. An intra-abdominal allograft location leads to higher risk of biopsy-related adverse events, such as bleeding or bowel injury [48]. (iii) The size mismatch between an allograft from an adult donor and the smaller pediatric recipient requires creative surgical approaches for allograft placement. Therefore, the anatomy of allograft and vessels is highly variable [49], which increases the risk of vascular injury and bleeding complications during biopsy. (iv) The excess functional capacity of a large adult kidney in a small pediatric body can mask substantial rejection by maintaining stable creatinine levels in children who receive an adult kidney. For this reason and since rejection occurs in up to 25 % of patients, biopsies are often done according to a protocol or with minimal or no changes in creatinine [50].

Macrophages play a critical role in transplant rejection [18, 51–54]. Macrophages are key inflammatory mediators of the innate immune response that contribute to both acute and chronic allograft rejection through a variety of mechanisms [52, 53]. Macrophages are attracted to sites of immune complex formation by complement fragments (*e.g.*, C5a) and specific cytokines/chemokines [55]. In the transplant, the macrophages are activated by IFN-γ (produced by T cells or NK cells) and TNF-α (produced by APCs), which leads to a pro-inflammatory cascade with production of reactive oxygen species, progressive transplant injury, and ultimately, graft rejection [53].

Previous pre-clinical studies demonstrated significant iron oxide enhancement of rejecting allografts in animal models. Histologic correlations in these models showed that the observed MR signal changes at 24–96 h post-USPIO injection were due to nanoparticle accumulation in prevalent macrophages in the transplant [56]. The iron oxide-induced MRI enhancement correlated with rejection scores according to the Banff classification [57, 58].

One study has investigated renal allograft rejection in human adult patients with iron oxide-enhanced MRI: Hauger et al. [16] investigated two patients with histologically confirmed renal allograft rejection and macrophage infiltration. These allografts demonstrated a minor signal loss at 72 h after infusion of the USPIO ferumoxtran-10 (Sinerem/Combidex).

In order to maximize the sensitivity of our imaging approach, we used MR scanners with high magnetic field strength (3 Tesla), applied iron-sensitive MRI sequences, and relatively higher iron oxide doses (5 mg Fe/kg). Nonetheless, we did not notice any T2* shortening, but rather T2* prolongation on   24 h delayed postcontrast scans in rejecting allografts in our study. This is likely because in our clinic, rejection is noticed early and severe, advanced rejections are rare. Our patients are followed closely and with routine biopsies to detect a potential immune reaction in its earliest stages, when it can be successfully treated with immune suppressing therapy [16]. Previously described cases of USPIO-enhancing transplants showed massive immune cell infiltrations, a scenario less commonly observed in

our clinic. Our observation of T2* prolongation in rejected allografts can be explained by histopathologically observed glomerular vasospasm and edema, which lead to an impaired organ perfusion [9, 59, 60]. This is in agreement with studies using BOLD MRI to detect acute allograft rejections [36, 37, 40, 42, 44–46].

Our data are in accordance with studies by Xiao et al. [40] who demonstrated that the medulla to cortex (M/C) T2* ratio increased significantly in patients undergoing acute renal allograft rejection. Likewise, Park et al. [42] found that medullary T2* values were significantly higher in cases of acute allograft rejection than in non-rejecting allografts and Sadowski et al. [37] demonstrated an increase in medullary T2* and medullary blood flow on gadolinium chelate-enhanced perfusion imaging in allografts undergoing acute rejection.

Ferumoxytol has a unique benefit in detecting differences in macrophage content on MRI. However, in our study, ferumoxytol did not detect increased quantities of macrophages but an impaired perfusion of rejecting allografts through its blood pool effect. This impaired allograft perfusion could be also detected with lower ferumoxytol doses than used in our study (thereby eliminating the blooming effect noted on our early postcontrast scans) and with other MRI techniques. Indeed, previous studies have also demonstrated reduced perfusion of rejecting renal allografts with Gadolinium chelates [12]. However, the advantage of ferumoxytol is that it can be applied irrespective of the renal function status [61], while gadolinium chelates can be only administered in patients with unimpaired renal function [62]. In addition, administration of gadolinium chelates is associated with a risk for gadolinium deposition in the brain [63]. On the other hand, ferumoxytol can induce rare, but life-threatening anaphylactic reactions, which led to a black box warning by the FDA [23]. Further work is needed to assess and improve the safety of ferumoxytol administrations.

We recognize several limitations of our study: Our studies were conducted in a limited number of patients. Pediatric patients are more difficult to recruit than adult patients, and fewer patients agree to participate in a trial compared to studies in adults. Since our findings unexpectedly reflect an impaired organ perfusion rather than macrophage infiltration, our findings have to be compared with other imaging tests which can measure kidney transplant perfusion such as ultrasound—the standard clinical imaging modality that allows a quick and inexpensive evaluation of vascular and morphological abnormalities [7]. Clinically applicable radiotracer-based approaches for detecting transplant rejection include relatively non-specific 2-deoxy-2-[^{18}F]fluoro-D-glucose-PET approaches [64], In-111-based leukocyte trafficking [65], and reporter gene imaging approaches [66]. These methods are relatively complicated and expensive, associated with significant radiation exposure, and are not specific enough to replace invasive biopsies. Several other approaches have been described for *in vivo* detection of leukocytes in organ transplants [67–71]. However, none of these have been translated to clinical applications to date.

Previous investigators have shown that acute tubular necrosis is manifested by vasoconstriction which reduces blood flow in the cortex with a shift of blood flow to the medulla [72, 73]. This and other pathologies, which lead to decreased organ perfusion, must be considered in the differential diagnosis.

Conclusion

Allografts undergoing acute rejection show prolonged T2* values on ferumoxytol-enhanced MR images compared to non-rejecting allografts. This may be attributable to reduced perfusion and increased edema in rejecting allografts. Surprisingly, rejecting allografts did not show significant ferumoxytol retention or macrophage phagocytosis on delayed MR images and histopathology in our series, presumably because rejection was noticed at a very early stage.

Supplementary Material

Refer to Web version on PubMed Central for supplementary material.

Acknowledgments.

References

1. Thiruchelvam PT, Willicombe M, Hakim N et al. (2011) Renal transplantation. Br Med J 343:d7300 [PubMed: 22084316]

2. Magee JC, Bucuvalas JC, Farmer DG et al. (2004) Pediatric transplantation. Am J Transplant 4(Suppl 9):54–71 [PubMed: 15113355]

3. McEnery PT, Stablein DM, Arbus G, Tejani A (1992) Renal transplantation in children. A report of the north American pediatric renal transplant cooperative study. N Engl J Med 326:1727–1732 [PubMed: 1594014]

4. Ogura Y, Krams SM, Martinez OM et al. (2000) Radiolabeled Annexin V imaging: diagnosis of allograft rejection in an experimental rodent model of liver transplantation 1. Radiology 214:795–800 [PubMed: 10715048]

5. Martins F, Souza S, Gonçalves R et al. (2004) Preliminary results of [^{99m}Tc] OKT3 scintigraphy to evaluate acute rejection in renal transplants. Transplant Proc 36:2664–2667 [PubMed: 15621118]

6. De Souza SL, Da Fonseca LB, Gonçalves RT et al. (2004) Diagnosis of renal allograft rejection and acute tubular necrosis by 99mTc-mononuclear leukocyte imaging. Transplant Proc 36:2997–3001 [PubMed: 15686680]

7. Cosgrove DO, Chan KE (2008) Renal transplants: what ultrasound can and cannot do. Ultrasound Q 24:77–87 [PubMed: 18528243]

8. Bashir MR, Jaffe TA, Brennan TV et al. (2013) Renal transplant imaging using magnetic resonance angiography with a nonnephrotoxic contrast agent. Transplantation 96:91–96 [PubMed: 23680931]

9. Wentland AL, Sadowski EA, Djamali A et al. (2009) Quantitative MR measures of intrarenal perfusion in the assessment of transplanted kidneys: initial experience. Acad Radiol 16:1077–1085 [PubMed: 19539502]

10. Laissy J-P, Idée J-M, Fernandez P et al. (2006) Magnetic resonance imaging in acute and chronic kidney diseases: present status. Nephron Clin Pract 103:c50–c57 [PubMed: 16543756]

11. Szolar DH, Preidler K, Ebner F et al. (1997) Functional magnetic resonance imaging of human renal allografts during the post-transplant period: preliminary observations. Magnet Reson Imaging 15(7):727–735

12. Kalb B, Martin DR, Salman K et al. (2008) Kidney transplantation: structural and functional evaluation using MR Nephrourography. J Magnet Reson Imaging 28:805–822

13. Wu YL, Ye Q, Eytan DF et al. (2013) Magnetic resonance imaging investigation of macrophages in acute cardiac allograft rejection after heart transplantation. Circ Cardiovasc Imaging 6:965–973 [PubMed: 24097421]

14. Kriz J, Jirák D, Girman P et al. (2005) Magnetic resonance imaging of pancreatic islets in tolerance and rejection. Transplantation 80:1596–1603 [PubMed: 16371931]

15. Chae EY, Song EJ, Sohn JY et al. (2010) Allogeneic renal graft rejection in a rat model: in vivo MR imaging of the homing trait of macrophages 1. Radiology 256:847–854 [PubMed: 20720071]

16. Hauger O, Grenier N, Deminère C et al. (2007) USPIO-enhanced MR imaging of macrophage infiltration in native and transplanted kidneys: initial results in humans. Europ Radiol 17:2898–2907

17. Ricardo SD, van Goor H, Eddy AA (2008) Macrophage diversity in renal injury and repair. J Clin Invest 118:3522–3530 [PubMed: 18982158]

18. Magil AB (2009) Monocytes/macrophages in renal allograft rejection. Transplant Rev 23:199–208

19. Tinckam KJ, Djurdjev O, Magil AB (2005) Glomerular monocytes predict worse outcomes after acute renal allograft rejection independent of C4d status. Kidney Int 68:1866–1874 [PubMed: 16164665]

20. Corot C, Robert P, Idee JM, Port M (2006) Recent advances in iron oxide nanocrystal technology for medical imaging. Adv Drug Deliv Rev 58:1471–1504 [PubMed: 17116343]

21. Daldrup-Link HE, Golovko D, Ruffell B et al. (2011) MRI of tumor-associated macrophages with clinically applicable iron oxide nano-particles. Clin Cancer Res 17:5695–5704 [PubMed: 21791632]

22. Aghighi M, Golovko D, Ansari C et al. (2015) Imaging tumor necrosis with Ferumoxytol. PLoS One 10:e0142665 [PubMed: 26569397]

23. Muehe AM, Feng D, von Eyben R et al. (2015) Safety report of Ferumoxytol for magnetic resonance imaging in children and young adults. Investig Radiol 51:221–227

24. Levey AS, Stevens LA (2010) Estimating GFR using the CKD epidemiology collaboration (CKD-EPI) creatinine equation: more accurate GFR estimates, lower CKD prevalence estimates, and better risk predictions. Am J Kidnet Dis 55:622–627

25. AMAG Pharmaceuticals, Inc. (2009) Feraheme (ferumoxytol) package insert Lexington, MA

26. Balakrishnan VS, Rao M, Kausz AT et al. (2009) Physicochemical properties of ferumoxytol, a new intravenous iron preparation. Eur J Clin Investig 39:489–496 [PubMed: 19397688]

27. Bullivant JP, Zhao S, Willenberg BJ et al. (2013) Materials characterization of Feraheme/ferumoxytol and preliminary evaluation of its potential for magnetic fluid hyperthermia. Int J Mol Sci 14:17501–17510 [PubMed: 24065092]

28. Neuwelt EA, Hamilton BE, Varallyay CG et al. (2009) Ultrasmall superparamagnetic iron oxides (USPIOs): a future alternative magnetic resonance (MR) contrast agent for patients at risk for nephrogenic systemic fibrosis (NSF)? Kidney Int 75:465–474 [PubMed: 18843256]

29. Haas M, Sis B, Racusen LC et al. (2014) Banff 2013 meeting report: inclusion of C4d-negative antibody-mediated rejection and antibody-associated arterial lesions. Am J Transplant 14:272–283 [PubMed: 24472190]

30. Yang D, Ye Q, Williams M et al. (2001) USPIO-enhanced dynamic MRI: evaluation of normal and transplanted rat kidneys. Magn Reson Med 46:1152–1163 [PubMed: 11746582]

31. Ye Q, Yang D, Williams M et al. (2002) In vivo detection of acute rat renal allograft rejection by MRI with USPIO particles. Kidney Inter 61:1124–1135

32. McCullough BJ, Kolokythas O, Maki JH, Green DE (2013) Ferumoxytol in clinical practice: implications for MRI. J Magn Reson Imaging 37:1476–1479 [PubMed: 23097302]

33. Bashir MR, Bhatti L, Marin D, Nelson RC (2015) Emerging applications for ferumoxytol as a contrast agent in MRI. J Magn Reson Imaging 41:884–898 [PubMed: 24974785]

34. Pai A, Nielsen J, Kausz A et al. (2010) Plasma pharmacokinetics of two consecutive doses of ferumoxytol in healthy subjects. Clin Pharmacol Therap 88:237–242 [PubMed: 20592725]

35. Auerbach M, Ballard H (2010) Clinical use of intravenous iron: administration, efficacy, and safety. ASH Educ Program Book 2010:338–347

36. Thoeny HC, Zumstein D, Simon-Zoula S et al. (2006) Functional evaluation of transplanted kidneys with diffusion-weighted and BOLD MR imaging: initial experience 1. Radiology 241:812–821 [PubMed: 17114628]

37. Sadowski EA, Djamali A, Wentland AL et al. (2010) Blood oxygen level-dependent and perfusion magnetic resonance imaging: detecting differences in oxygen bioavailability and blood flow in transplanted kidneys. Magn Reson Imaging 28:56–64 [PubMed: 19577402]

38. Khalifa F, Abou El-Ghar M, Abdollahi B et al. (2013) A comprehensive non-invasive framework for automated evaluation of acute renal transplant rejection using DCE-MRI. NMR Biomed 26:1460–1470 [PubMed: 23775728]

39. Sharma RK, Gupta RK, Poptani H et al. (1995) The magnetic resonance renogram in renal transplant evaluation using dynamic contrast-enhanced MR imaging. Transplantation 59:1405–1409 [PubMed: 7770926]

40. Xiao W, Xu J, Wang Q et al. (2012) Functional evaluation of transplanted kidneys in normal function and acute rejection using BOLD MR imaging. Eur J Radiol 81:838–845 [PubMed: 21392910]

41. Vermathen P, Binser T, Boesch C et al. (2012) Three-year follow-up of human transplanted kidneys by diffusion-weighted MRI and blood oxygenation level-dependent imaging. J Magn Reson Imaging 35:1133–1138 [PubMed: 22180302]

42. Park SY, Kim CK, Park BK et al. (2012) Evaluation of transplanted kidneys using blood oxygenation level–dependent MRI at 3 T: a preliminary study. Am J Roentgenol 198:1108–1114 [PubMed: 22528900]

43. Xin-Long P, Jing-Xia X, Jian-Yu L et al. (2012) A preliminary study of blood-oxygen-level-dependent MRI in patients with chronic kidney disease. Magn Reson Imaging 30:330–335 [PubMed: 22244540]

44. Djamali A, Sadowski EA, Samaniego-Picota M et al. (2006) Noninvasive assessment of early kidney allograft dysfunction by blood oxygen level-dependent magnetic resonance imaging. Transplantation 82:621–628 [PubMed: 16969284]

45. Djamali A, Sadowski EA, Muehrer RJ et al. (2007) BOLD-MRI assessment of intrarenal oxygenation and oxidative stress in patients with chronic kidney allograft dysfunction. Am J Physiol Renal Physiol 292:F513–F522 [PubMed: 17062846]

46. Sadowski EA, Fain SB, Alford SK et al. (2005) Assessment of acute renal transplant rejection with blood oxygen level–dependent MR imaging: initial experience 1. Radiology 236:911–919 [PubMed: 16118170]

47. Bujok GJ, Misio ek H (2006) Choice of optimal anesthesia for transdermal kidney biopsy. Pediatr Anesth 16:596–597

48. Benfield MR, Herrin J, Feld L et al. (1999) SAFETY OF KIDNEY BIOPSY IN PEDIATRIC TRANSPLANTATION: a report of the controlled clinical trials in pediatric transplantation trial of induction therapy study Group1, 2. Transplantation 67:544–547 [PubMed: 10071025]

49. Donati-Bourne J, Roberts H, Coleman R (2014) Donor-recipient size mismatch in paediatric renal transplantation. J Transp Secur 67:544–547

50. Bunchman TE, Fryd DS, Sibley RK, Mauer SM (1990) Manifestations of renal allograft rejection in small children receiving adult kidneys. Pediatr Nephrol 4:255–258 [PubMed: 2400654]

51. Bergler T, Jung B, Bourier F et al. (2016) Infiltration of macrophages correlates with severity of allograft rejection and outcome in human kidney transplantation. PLoS One 11:e0156900 [PubMed: 27285579]

52. Wyburn KR, Jose MD, Wu H et al. (2005) The role of macrophages in allograft rejection. Transplantation 80:1641–1647 [PubMed: 16378052]

53. Mannon RB (2012) Macrophages: contributors to allograft dysfunction, repair or innocent bystanders? Curr Opin Organ Transplant 17:20–25 [PubMed: 22157320]

54. Chadban SJ, Wu H, Hughes J (2010) Macrophages and kidney transplantation. Semin Nephrol 30:278–289 [PubMed: 20620672]

55. Shushakova N, Skokowa J, Schulman J et al. (2002) C5a anaphylatoxin is a major regulator of activating versus inhibitory FcγRs in immune complex–induced lung disease. J Clin Invest 110:1823–1830 [PubMed: 12488432]

56. Zhang Y, Dodd SJ, Hendrich KS et al. (2000) Magnetic resonance imaging detection of rat renal transplant rejection by monitoring macrophage infiltration. Kidney Int 58:1300–1310 [PubMed: 10972694]

57. Beckmann N, Cannet C, Fringeli-Tanner M et al. (2003) Macrophage labeling by SPIO as an early marker of allograft chronic rejection in a rat model of kidney transplantation. Magn Reson Med 49:459–467 [PubMed: 12594748]

58. Beckmann N, Cannet C, Zurbruegg S et al. (2006) Macrophage infiltration detected at MR imaging in rat kidney allografts: early marker of chronic rejection? Radiology 240:717–724 [PubMed: 16837667]

59. Dempster W (1971) The nature of experimental second-set kidney transplant reaction: 2. The mimicking of the haemodynamic upset by pharmacological and other means. Br J Exper Pathol 52:172 [PubMed: 4325831]

60. Salaman J, Griffin PA (1983) Fine-needle intrarenal manometry: a new test for rejection in cyclosporin-treated recipients of kidney transplants. Lancet 322:709–711

61. Lu M, Cohen MH, Rieves D, Pazdur R (2010) FDA report: ferumoxytol for intravenous iron therapy in adult patients with chronic kidney disease. Am J Hematol 85:315–319 [PubMed: 20201089]

62. Golovko D, Sutton E, Daldrup-Link HE (2013) Magnetic resonance imaging of the Bone Marrow contrast Media for Bone Marrow Imaging. Magn Reson Imaging Bone Marrow 10.1007/174-2012-577

63. McDonald RJ, McDonald JS, Kallmes DF et al. (2015) Intracranial gadolinium deposition after contrast-enhanced MR imaging. Radiology 275:772–782 [PubMed: 25742194]

64. Heelan BT, Osman S, Blyth A et al. (1998) Use of 2-[^{18}F]fluoro-2-deoxyglucose as a potential agent in the prediction of graft rejection by positron emission tomography. Transplantation 66:1101–1103 [PubMed: 9808498]

65. Kuyama J, McCormack A, George AJ et al. (1997) Indium-111 labelled lymphocytes: isotope distribution and cell division. Eur J Nucl Med 24:488–496 [PubMed: 9142728]

66. Thölking G, Schuette-Nuetgen K, Kentrup D, Pawelski H, Reuter S (2016) Imaging-based diagnosis of acute renal allograft rejection. World J Transplant 6:174–182 [PubMed: 27011915]

67. George AJ, Bhakoo KK, Haskard DO et al. (2006) Imaging molecular and cellular events in transplantation. Transplantation 82:1124–1129 [PubMed: 17102760]

68. Ho C, Hitchens TK (2004) A non-invasive approach to detecting organ rejection by MRI: monitoring the accumulation of immune cells at the transplanted organ. Curr Pharm Biotechnol 5:551–566 [PubMed: 15579044]

69. Kondo I, Ohmori K, Oshita A et al. (2004) Leukocyte-targeted myocardial contrast echocardiography can assess the degree of acute allograft rejection in a rat cardiac transplantation model. Circulation 109:1056–1061 [PubMed: 14967733]

70. Dodd CH, Hsu HC, Chu WJ et al. (2001) Normal T-cell response and in vivo magnetic resonance imaging of T cells loaded with HIV transactivator-peptide-derived superparamagnetic nanoparticles. J Immunol Methods 256:89–105 [PubMed: 11516758]

71. Weller GE, Lu E, Csikari MM et al. (2003) Ultrasound imaging of acute cardiac transplant rejection with microbubbles targeted to intercellular adhesion molecule-1. Circulation 108:218–224 [PubMed: 12835214]

72. Nilsson L, Ekberg H, Fält K et al. (1994) Renal arteriovenous shunting in rejecting allograft, hydronephrosis, or haemorrhagic hypotension in the rat. Nephrol Dial Transplant 9:1634–1639 [PubMed: 7870354]

73. Nilsson L, Sterner G, Ekberg H (1999) Presence of arteriovenous shunting in transplanted but not in native single kidney in the rat. Scand J Urol Nephrol 33:363–367 [PubMed: 10636574]
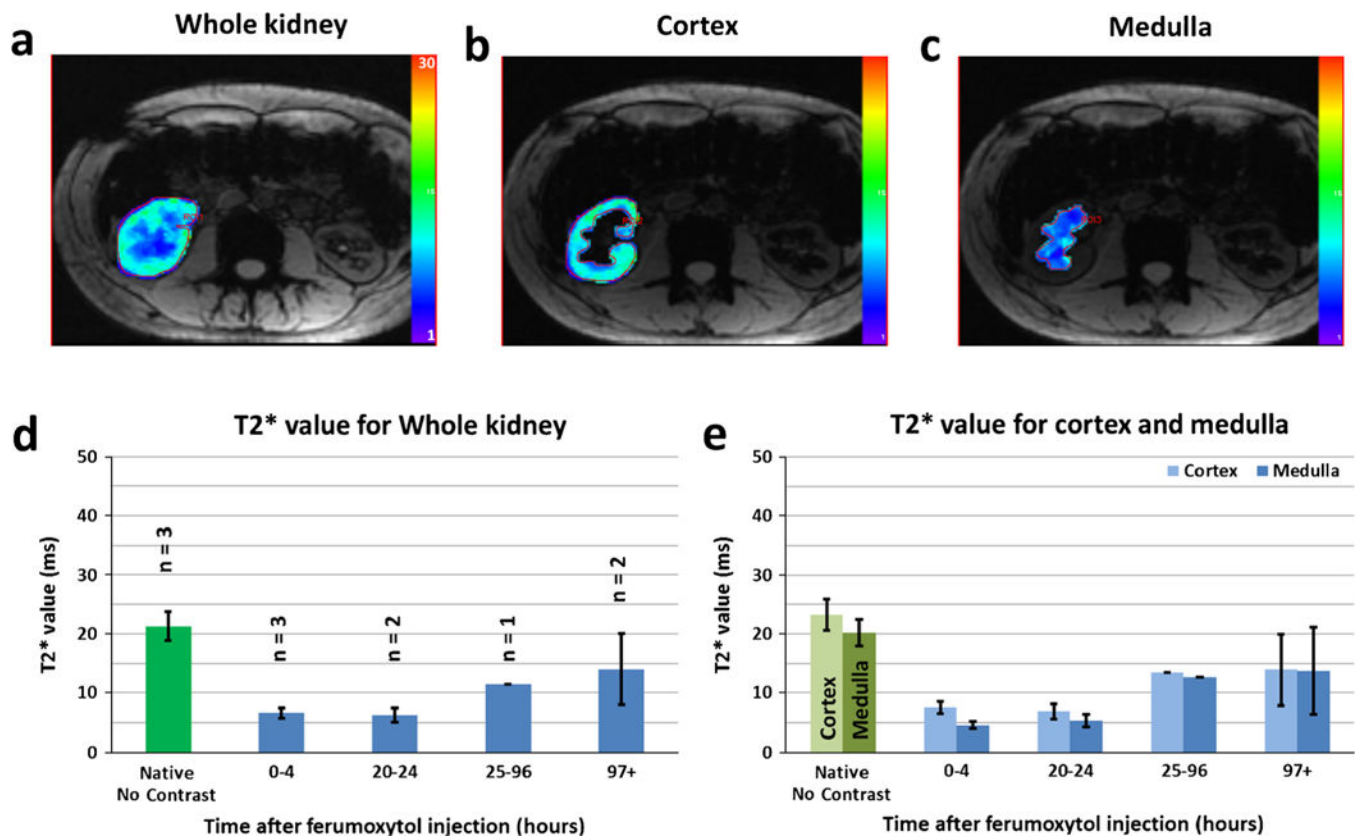
Fig. 1.
T2* signal kinetic of native kidneys. T2* relaxation time maps, superimposed on axial T2*-weighted SPGR images of **a** whole kidney, **b** cortex, and **c** medulla of a native kidney at 20 h p.i. of ferumoxytol. Corresponding T2* relaxation times of **d** whole kidney cortex (*blue*) and **e** medulla on pre-contrast scans (*green*) and at different time points after intravenous ferumoxytol injection. Data are displayed as mean data with standard deviations (number of kidneys per group indicated).
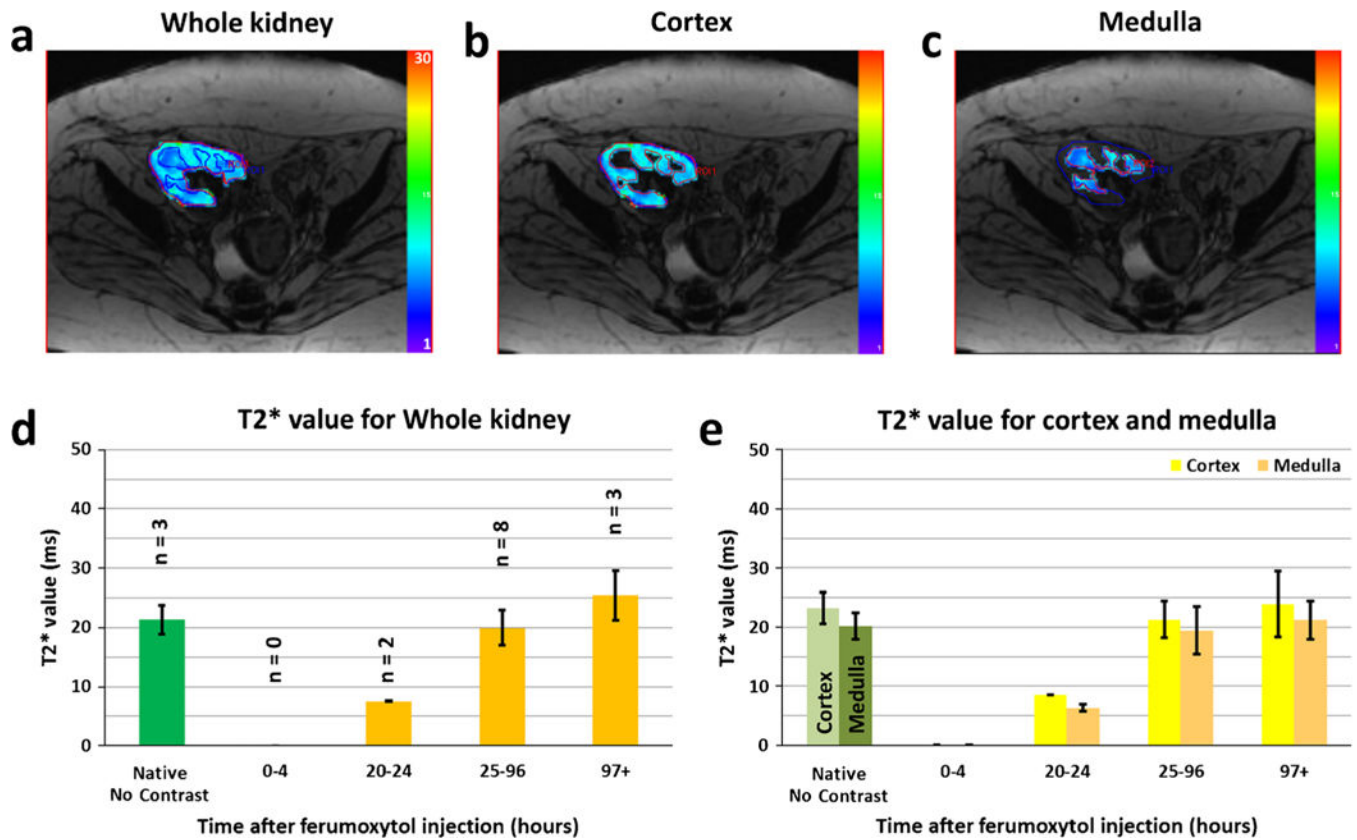
Fig. 2.
T2* signal kinetic of non-rejecting renal allografts. T2* relaxation time maps, superimposed on axial T2*-weighted SPGR images of **a** whole kidney, **b** cortex, and **c** medulla of a non-rejecting allograft at 20 h p.i. Corresponding T2* relaxation times of **d** whole kidney pre-contrast (*green*) as well as the whole allograft (*yellow*), and **e** cortex and medulla at different time points after intravenous ferumoxytol injection. Data are displayed as mean data and standard deviation, with number of kidneys per group indicated.
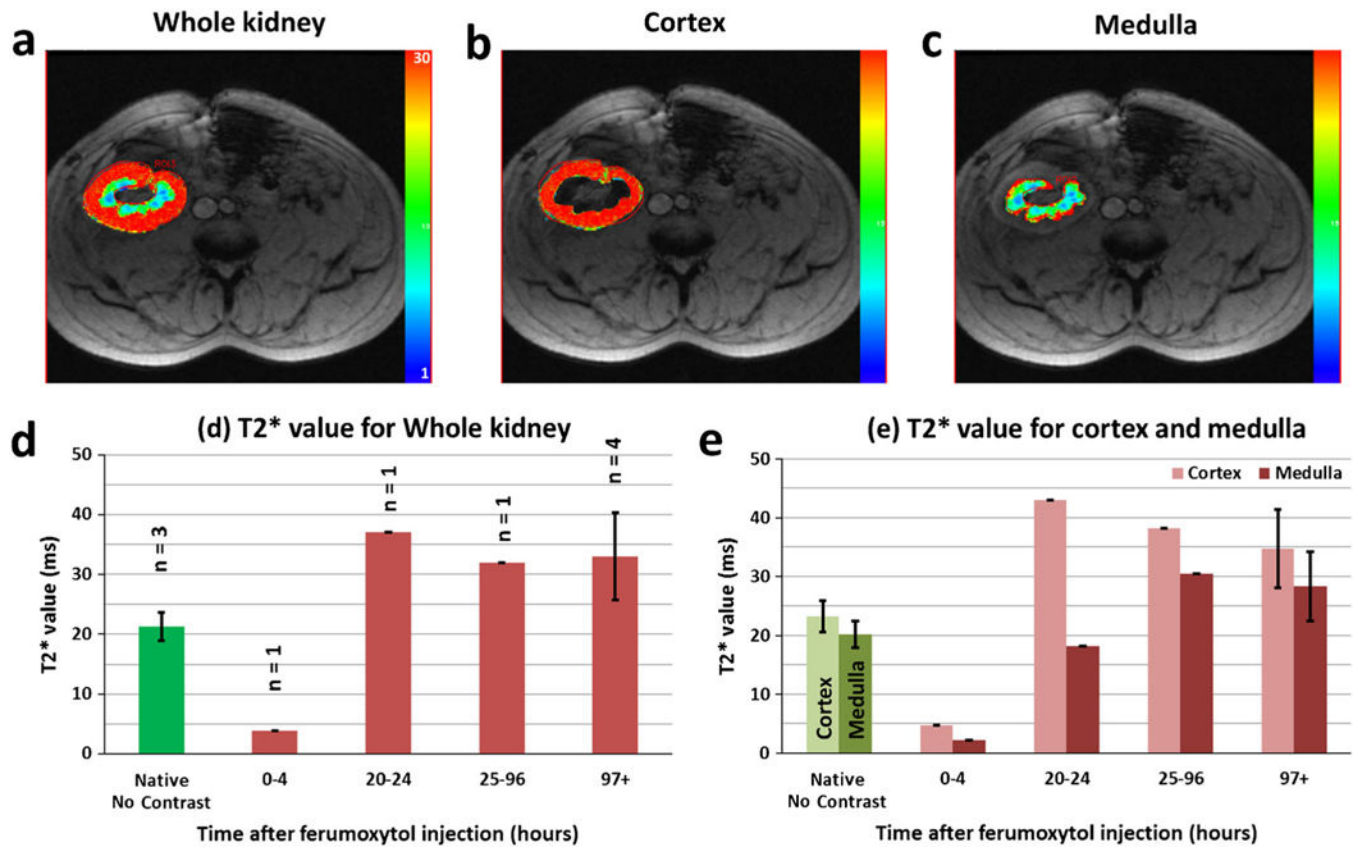
Fig. 3.

T2* signal kinetic of renal allografts undergoing acute rejection. Color-coded T2* relaxation time maps, superimposed on axial T2*-weighted SPGR of **a** whole kidney, **b** cortex, and **c** medulla of a representative rejecting kidney at 20 h p.i. Corresponding T2* relaxation times of **d** native kidneys pre-contrast (*green*) as well as rejecting allografts (*red*), and **e** cortex and medulla at different time points after intravenous ferumoxytol injection. Data are displayed as mean data and standard deviation, with number of kidneys per group indicated.
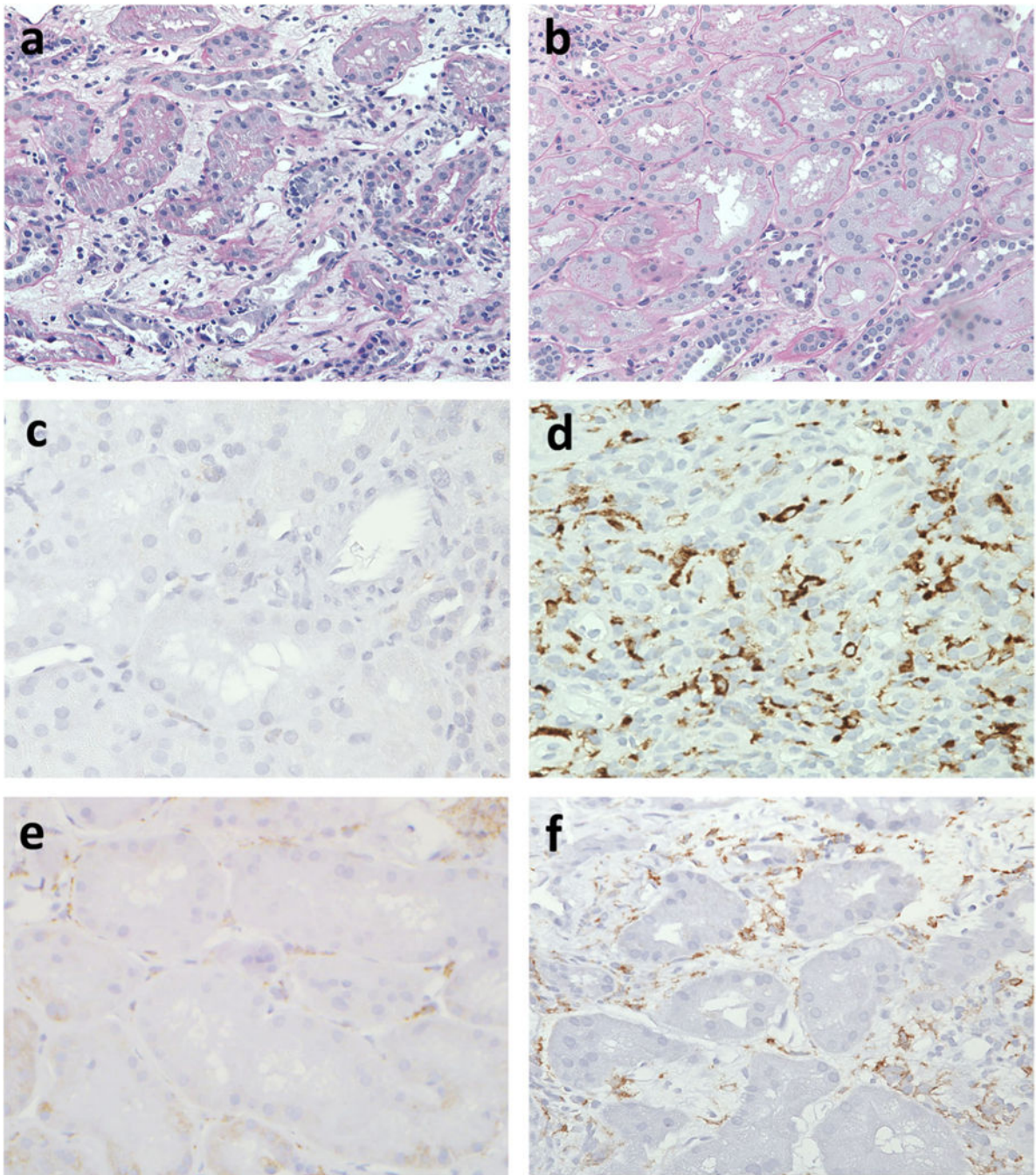
Fig. 4.

CD163 histopathology (*brown stain*) of representative allografts. **a** Normal kidney devoid of inflammation and edema. The non-atrophic tubules are back to back and the interstitium is barely visualized at ×200 magnification. **b** An acutely rejecting kidney shows interstitial expansion by edema characterized by loose myxoid stroma. Interstitial inflammation and tubulitis typical of T cell-mediated rejection are seen at ×200 magnification. **c** A non-rejecting allograft with no evidence of macrophage infiltration (negative CD163 stain) at ×400 magnification. **d** A non-rejecting allograft with parenchymal scarring possibly due to

reflux nephropathy showing numerous CD163-positive macrophages at ×400 magnification. **e** An allograft undergoing rejection with minimal macrophage infiltration at ×400 magnification. **f** An allograft with histological features of both tubulointerstitial T cell-mediated and antibody-mediated acute rejection showing numerous CD163-positive macrophages within the interstitium and peritubular capillaries at ×400 magnification.
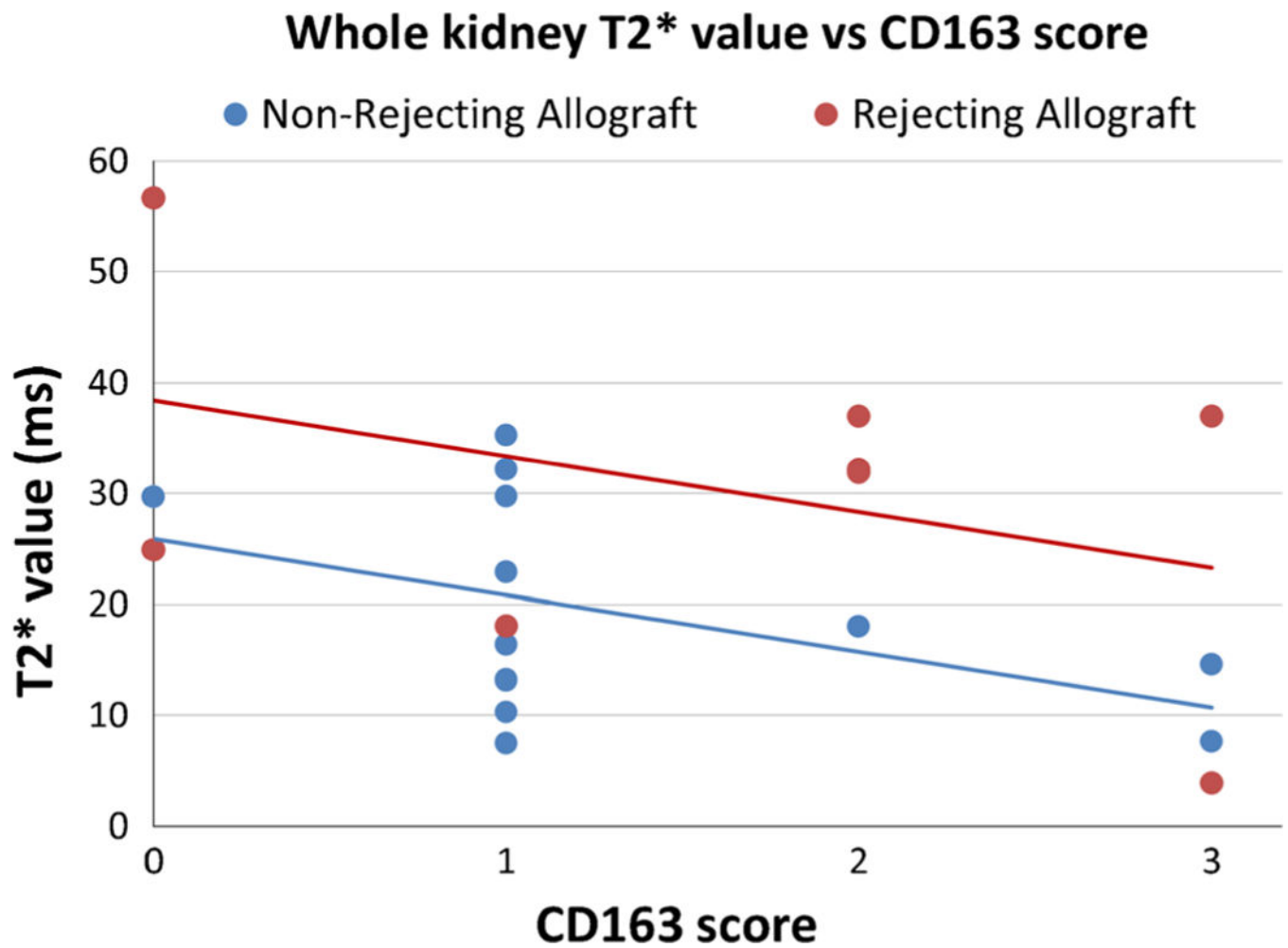
Fig. 5.
Scatter plot of T2* relaxation time *versus* CD163 score of non-rejecting and rejecting allografts. The correlation between T2* value and CD163 score is not significant for patients with non-rejecting ($p = 0.12$) or rejecting allografts ($p = 0.34$).
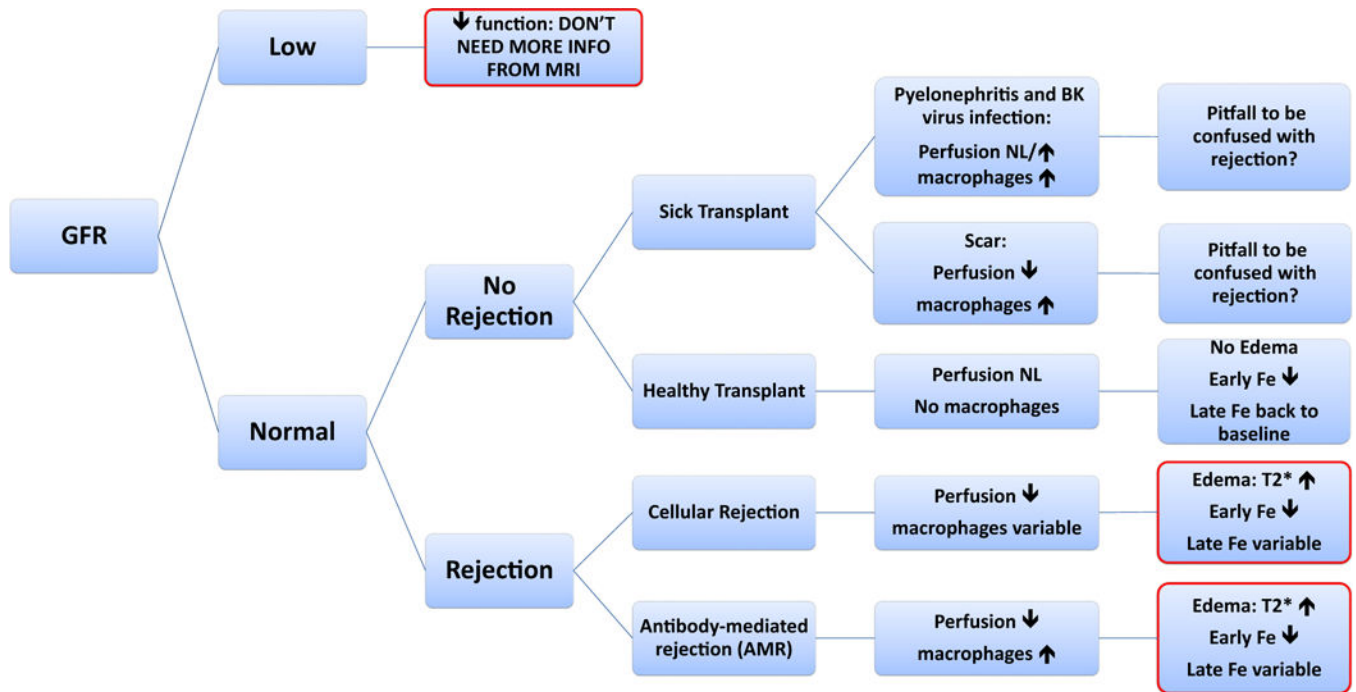
Fig. 6.
Diagnostic decision chart for ferumoxytol (Fe) enhancement patterns of allografts with different physiological and pathological conditions. *NL* normal.

Table 1.

List of allograft patients with their rejection state, CD163 score, mean T2* value over whole kidneys, medulla and cortex, serum creatinine concentration, and GFR

Patient no.	Rejection state	CD163 score 0–3[a]	MRI time point h p.i.	T2[a] (whole)	T2[a] (cortex)	T2[a] (medula)	Creatinine (mg/dl)	GFR (ml/min/1.73 m^2)
1	No	1	97+	22.89	18.80	14.01	1.0	108
2	No	0	49–96	29.69	22.36	27.62	0.5	150
3[b]	No	3	49–96	14.66	18.27	13.22	2.2	42
4	No	1	49–96	13.28	13.30	16.50	1.0	124
5	No	1	25–48	16.45	19.98	10.48	1.5	67
6	No	1	49–96	10.27	10.33	10.64	1.2	64
7	No	1	25–48	13.17	16.06	9.34	1.0	82
8	No	2	97+	18.07	15.40	21.90	0.9	92
9	No	1	49–96	32.17	35.20	44.97	0.8	112
10[b]	No	3	20–24	7.62	8.47	7.10	1.2	66
11	No	1	49–96	29.72	34.86	22.65	1.3	60
12	No	1	20–24	7.48	8.55	5.50	1.1	98
13	No	1	97+	35.27	37.38	27.60	0.8	105
14[c]	Yes	0	97+	24.91	24.42	20.93	1.8	62
14	Yes	0	97+	56.70	56.40	48.70	1.8	62
15[c]	Yes	3	20–24	37.00	43.00	18.16	1.5	68
15	Yes	2	20–24	37.00	43.00	18.16	1.5	68
16	Yes	2	97+	32.18	35.10	23.51	1.2	87
17[c]	Yes	1	97+	18.13	23.09	20.08	2.0	55
17	Yes	2	49–96	31.93	38.10	30.40	4.5	21
18	Yes	3	0–3	3.87	4.65	2.15	3.2	20

[a] 0: neg; 1: focal occasional + cells <25 % sample; 2: >10/hpf involving at least 25 % of sample; 3: >10/hpf involving >50 % of sample

[b] Patient #3 had allograft biopsy with parenchymal scarring and patient #10 had BK nephropathy

[c] Patient #14 had two MRI scans. Patients #15 and #17 had two biopsies and two MRI scans

Table 2.

Previous contrast-enhanced MRI investigations of renal allograft rejection

Study	Year	Patients	MRI sequence	Field strength	Contrast agent	Dose	Imaging time point
Khalifa et al. [38]	2013	50 patients: 27 stable kidney, 23 rejection	DCE-MRI: T1w GRE	1.5 T	Gadoteric acid (Dotarem 0.5 mmol/ml)	0.2 ml/kg	3 s/fr × 80fr p.i.
Bashir et al. [8]	2013	16 kidney transplant	MRA, T1w DCE, pre- and post-contrast T1w		Ferumoxytol	253 ± 48 mg	T1w-DCE: 3–4 s/fr during IV bolus injection
Sadowski et al. [37]	2010	17 patients with recently transplanted kidneys	BOLD MRI: T2*w multi-GRE Perfusion MRI: T2*w EPI	1.5 T	Gadodiamide	0.1 mmol/kg at a rate of 3cm³/s	Multi-GRE pre-contrast. EPI: 1 s/fr × 180fr during injection
Wentland et al. [9]	2009	21 patients with recently transplanted kidneys	Perfusion MRI: T2*w EPI Post-contrast T1w GRE	1.5 T	Gadodiamide	0.1 mmol/kg	EPI: 1 s/fr × 160fr during injection
Hauger et al. [16]	2007	12 patients: 7 rapidly progressive renal failure, 5 renal graft rejection	T1w SE, T2w TSE and T2*w GE-EPI	1.5 T	Ferumoxtran-10 (Sincerem) USPIO	1.7–2.6 mg of iron/kg	Before, immediate and 72 h p.i.
Szolar et al. [11]	1997	31 patients: 8 normal allograft, 23 allograft with ATN and/or AAR	T1w TSE; T2w TSE; Perfusion MRI: fGRE	1.5 T	Gd-DTPA	0.1 mmol/kg	Pre-contrast TSE; During injection fGRE 3 s/fr × 60fr
Sharma et al. [39]	1995	17 patients: 5 normal allografts, 5 acute rejection, 7 cyclosporine nephrotoxicity	T1w Turbo-FLASH	2 T	Gd-DTPA	2 ml (0.5 mmol/ml)	Pre-contrast, 1 s/ fr × 128fr, 10s/ fr × 6

Table 3.

Previously reported T2* measurements of renal allografts and native kidneys

Study	Year	Patients	MRI sequence	Field strength	T2*: Healthy volunteer	T2*: Normal allograft	T2*: acute rejection
Xiao et al. [40]	2012	122 patients: 20 volunteers, 72 normal allograft, 21 acute rejection	16 echo Mgre	1.5 T	M: 56.43 ms C: 72.3 ms	M: 55.77 ms C: 68.92 ms	M: 78.86 ms C: 88.5 ms
Vermathen et al. [41]	2012	9 patients with renal allografts	12 echo mGRE	1.5 T		M: 66.67 ms C: 82.64 ms	
Park et al. [42]	2012	22 patients: 10 volunteers, 8 normal allograft, 4 acute allograft rejection	FFE with 3 echos	3 T	M: 31.85 ms C: 65.79 ms	M: 31.45 ms C: 68.97 ms	M: 44.44 ms C: 76.92 ms
Xin-Long et al. [43]	2012	26 patients:15 healthy, 11 chronic kidney disease	8 echo mGRE	3 T	M: 50.05 ms C: 62.38 ms		
Thoeny et al. [36]	2006	30 patients: 15 volunteer, 15 stable kidney allograft	12 echo mGRE	1.5 T	M: 65.36 ms C: 86.96 ms	M: 77.52 ms C: 90.91 ms	
Djamali et al. [44]	2006	23 patients: 5 normal transplants, 18 biopsy-proven acute allograft dysfunction	16 echo mGRE	1.5 T		41.15 ms	60.24 ms
Djamali et al. [45]	2007	19 patients: 9 healthy volunteers, 10 kidney-transplant recipients with chronic allograft nephropathy	16 echo mGRE	1.5 T		48.31 ms	62.89 ms
Sadowski et al. [46]	2005	20patients: 6 normal transplants, 8 h biopsy-proved rejection, 6 biopsy-proved ATN	16 echo mGRE	1.5 T		41.84 ms	63.29 ms